WS$_2$ based 523 MHz mode-locked erbium-doped fiber laser for microwave photonic application

Kan Wu,[1,6] Xiaoyan Zhang,[2,3] Jun Wang,[2,3,4,5] (iD) Xing Li,[1] Weiwen Zou,[1] and Jianping Chen[1]

[1] *Shanghai Institute for Advanced Communication and Data Science, State Key Laboratory of Advanced Optical Communication Systems and Networks, Department of Electronic Engineering, Shanghai Jiao Tong University, Shanghai 200240, China*

[2] *Laboratory of Micro-Nano Photonic and Optoelectronic Materials and Devices, Key Laboratory of Materials for High-Power Laser, Shanghai Institute of Optics and Fine Mechanics, Chinese Academy of Sciences, Shanghai 201800, China*

[3] *Center of Materials Science and Optoelectronic Engineering, University of Chinese Academy of Sciences, Beijing 100049, China*

[4] *CAS Center for Excellence in Ultra-intense Laser Science (CEULS), Shanghai 201800, China*

[5] *jwang@siom.ac.cn*

[6] *kanwu@sjtu.edu.cn*

Abstract: Microwave photonics is an important application for mode-locked lasers and requires the lasers to have high repetition rate and relatively low timing jitter. Although many mode-locked lasers based on two-dimensional (2D) materials have been reported, their applications in high-quality microwave photonics have not been achieved yet. We demonstrate a linear-cavity mode-locked Erbium-doped fiber laser with tungsten disulfide (WS$_2$) saturable absorber (SA). By optimizing the WS$_2$ SA fabrication, SA with low loss and moderate modulation depth is obtained. The laser based on this WS$_2$ SA is demonstrated to have a fundamental repetition rate of 523 MHz, a central wavelength of 1558.6 nm, a 3-dB bandwidth of 7.4 nm and a timing jitter of 28 fs. With this laser, microwave photonic application of frequency synthesis is obtained with a tuning range up to 10 GHz and an extinction ratio greater than 60 dB in the whole range. We believe this is the first work that utilizes a 2D material SA based mode-locked laser for high-quality microwave photonic applications. This work indicates the potential of 2D material SA for high-speed and high-precision photonic and microwave systems.

1.   Introduction

In recent years, novel two-dimensional (2D) materials have attracted intense interest for their abundant photonic properties [1,2]. Saturable absorption is one of the most widely investigated properties. Many works of mode-locked and Q-switched lasers based on 2D material saturable absorber (SA) have been reported [2,3]. Briefly, these 2D materials include graphene [2,4–14], graphene oxide [15,16], topological insulators [17–19], transition metal dichalcogenides [20–31], black phosphorus [32–37] and many other new nanomaterials [38–43]. The laser operation wavelengths have been extended from visible to mid-IR region [33,37,44,45]. Gigahertz-level high repetition rates of mode-locked lasers have been demonstrated [7,18]. Moreover, all-optical signal processing based on various nanomaterials have also been investigated. Optical phase shifter [46–48], modulator [49–51], switch [47,48,52] and autocorrelator [53] are reported using thermo-optic effect, saturable absorption and other nonlinear effect.

Meanwhile, for many high-speed and high-precision photonic applications such as photonic analog-to-digital convertor, a mode-locked fiber laser with high fundamental repetition rate and low timing jitter is required [54]. High repetition rate enables high processing speed [55] and low timing jitter allows high processing precision [56]. Compared with harmonic mode

locking, fundamental mode locking has a single pulse propagating in the cavity and avoids the discrepancy among multiple pulses in the cavity, which usually leads to better spectral purity and lower noise level. Also, operation wavelength near 1550 nm is preferred because mature optical devices for telecommunications can be directly used to build the system. Therefore, a fundamentally mode-locked fiber laser near 1550 nm with high repetition rate and low jitter is desired. A few such lasers with nanomaterial SA have been reported including carbon nanotubes [57], graphene [7] and MoS_2 [29]. Other works based on III-V semiconductor SA and nonlinear polarization evolution have reached 1 GHz [58] and 517 MHz [59] near 1550 nm, respectively. Although graphene has been shown a successful SA for mode locking operation. It has not been utilized for microwave photonic application yet. Also it is still unclear whether other 2D material SAs can achieve comparable performance in high-repetition-rate and low-jitter mode locking. Demonstration of high-performance laser with 2D materials other than graphene can extend the applications of various novel 2D materials for high-speed and high precision microwave photonics systems.

In this paper, we report a 523 MHz mode-locked Erbium-doped fiber laser with tungsten disulfide (WS_2) saturable absorber and its application in microwave photonics. The WS_2 nanosheets are embedded in polyvinyl alcohol (PVA) thin film to form an SA. The SA has a modulation depth of 3.4% and a saturation intensity of ~200 MW/cm^2. The WS_2-PVA SA is incorporated into a fiber linear cavity and the fundamental mode locking operation is achieved. The laser has a repetition rate of 523.1 MHz, a central wavelength of 1558.6 nm, a bandwidth of 7.4 nm and a timing jitter of 28 fs (1 kHz – 1 MHz). Moreover, microwave photonic application of high-purity microwave frequency synthesis using this laser has been demonstrated. Frequency up to 10.46 GHz is obtained and all the generated frequencies have an extinction ratio ≥60 dB. We believe this is the first work that utilizes a 2D material saturable absorber based mode-locked laser for high-quality microwave photonic application. This work indicates the potential of 2D material SA for high-speed and high-precision photonic and microwave systems.

2.　Saturable absorber fabrication

The WS_2 saturable absorber is a key component for the high-repetition-rate fiber laser. Our previous work has shown that saturable absorber with fast decay time can improve the noise properties of mode-locked lasers by suppressing the noise coupling inside the cavity [60]. Compared with conventional III-V semiconductor based saturable absorber, 2D materials typically exhibit faster decay process and thus have the potential to enable low-noise mode locking operation. However, due to the fabrication process, the transmission loss of 2D material SA (e.g., absorption, scattering, coupling, etc.) is not very good compared with the III-V semiconductor SA. This drawback counteracts the advantage of fast decay of 2D materials. In this work, we further optimize the fabrication process of WS_2 SA to reduce the transmission loss while maintaining a moderate modulation depth.

The fabrication of WS_2 SA includes two steps: preparation of WS_2 nanosheets and fabrication of WS_2-PVA thin-film SA. Liquid-phase exfoliation (LPE) method can produce large-volume nanosheets with high quality. Therefore, we choose LPE method to prepare WS_2 nanosheets from commercial WS_2 powders. The WS_2 powders are exfoliated to few-layer nanosheets by ultrasonic processing in deionized water with sodium cholate (SC) as surfactant. Typically, 5 mg/mL WS_2 powders are dispersed in 1.5 mg/mL SC aqueous solution and sonicated for 1 hour using a horn probe sonic tip (VibraCell CVX; 750 W) with 38% output power. Then the mixture is centrifuged at 3000 rpm for 90 minutes to separate nanosheets and un-exfoliated flakes. The upper part of the dispersion is collected by a pipette and the WS_2 nanosheet dispersions are obtained. The un-exfoliated flakes are the main reason for scattering loss, so the centrifugation step is processed very carefully to remove these flakes. The existence of WS_2 nanosheets in the dispersions is confirmed by transmission electron microscope (TEM), as shown in Fig. 1(a). The concentration

of WS_2 nanosheet dispersions is ~0.016 mg/ml. WS_2 nanosheets with the size of a few hundreds of nanometers can be observed. It is then mixed with PVA aqueous solution and dried on a glass plate at room temperature to form thin film, as shown in Fig. 1(b). The WS_2-PVA thin film is finally cut into ~2×2 mm pieces and transferred onto fiber end to function as an SA, as shown in Fig. 1(c). The Raman spectrum of WS_2-PVA SA is measured at an excitation wavelength of 532 nm and shown in Fig. 1(d) to confirm the existence of WS_2. The frequency difference between the in-plane vibrational mode E^1_{2g} (354.7 cm^{-1}) and the out-of-plane vibrational mode A_{1g} (420.7 cm^{-1}) is ~66.0 cm^{-1}. It is known that this frequency difference is related to layer number of WS_2 nanosheets due to the anomalous lattice vibrations of the layered 2H-WS_2. The value of 66.0 cm^{-1} indicates the number of monolayers to be 3-5 [61]. The results demonstrate that high quality 2D WS_2-PVA thin film is fabricated.
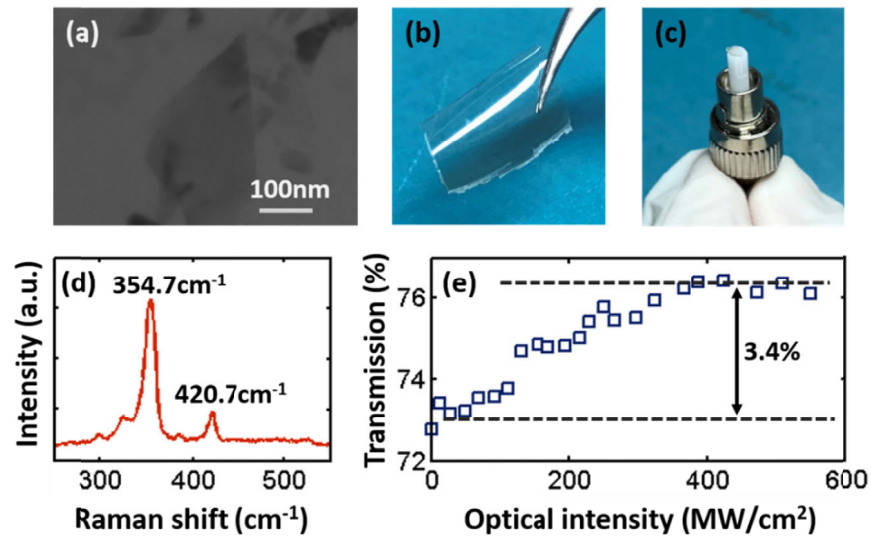

Fig. 1. (a) TEM image of WS_2 nanosheets. (b) Photo of WS_2-PVA thin film. (c) Photo of WS_2-PVA SA transferred on fiber end. (d) Raman spectrum. (e) Saturable absorption.

The saturable absorption of the WS_2-PVA SA has also been characterized, as shown in Fig. 1(e). A typical two-arm system is used. The output of a homemade 1550-nm mode-locked laser (37 MHz repetition rate, ~250 fs pulse duration and ~1 kW pulse peak power) is divided to two arms with 99:1 power split ratio. Light with 1% power in one arm is directly measured by a power meter as reference. Light with 99% power in the other arm is injected in to the SA and then measured by a second power meter. By comparing the readings in two power meters, the nonlinear transmission property of SA, i.e. saturable absorption, can be obtained. More details of the two-arm system can refer to our previous work [3]. In Fig. 1(e), the transmission (absorption) of the SA increases (decreases) with the increase of input optical intensity, which clearly indicates the saturable absorption of the sample. The modulation depth is ~3.4%. The saturation intensity is ~200 MW/cm^2. The nonsaturable loss is ~24% which is due to the scattering and absorption of the residual WS_2 flakes and PVA thin film.

## 3. High-repetition-rate mode-locked laser

The experimental setup of the mode-locked fiber laser is shown in Fig. 2(a). The linear cavity design is adopted to allow short cavity length and high fundamental repetition rate. The cavity consists of ~11 cm Erbium-doped fiber (EDF, LIEKKI Er80 8/125) and ~8.5 cm standard single mode fiber (SMF). The EDF has an anomalous dispersion of ~−22 ps^2/km. The net cavity

dispersion is ~-0.0043 ps^2 and the laser is designed to operate in the soliton mode-locking regime. On the left end of the cavity, the EDF is spliced with a short piece of SMF and glued to a standard ceramic ferrule, as shown in Fig. 2(b). The ferrule end facet is polished and connected with a coated fiber FC/PC connector using a fiber adapter. This FC/PC connector has a dichroic coating with 10% transmission near 1550 nm as output coupler and high transmission at 980 nm for pump coupling. On the right end of the cavity, the WS$_2$-PVA SA is sandwiched between a fiber ferrule and a dielectric mirror, as shown in Fig. 2(c). The fiber ferrule has a high reflection coating at 980 nm ($\sim$95%) to improve the pumping efficiency and protect the SA from being damaged by the residual pump. The dielectric mirror has a high reflection near 1550 nm ($\sim$98%). The cavity birefringence is adjusted by a compact fiber polarization controller (PC). Outside the cavity, a 980/1550 wavelength division multiplexer (WDM) is used to combine the 976-nm pump light and the laser output near 1556 nm. The laser output is characterized by optical spectrum analyzer (Yokogawa AQ6370C), autocorrelator (Femtochrome 103XL) and signal source analyzer (Rohde & Schwarz FSUP50), etc.
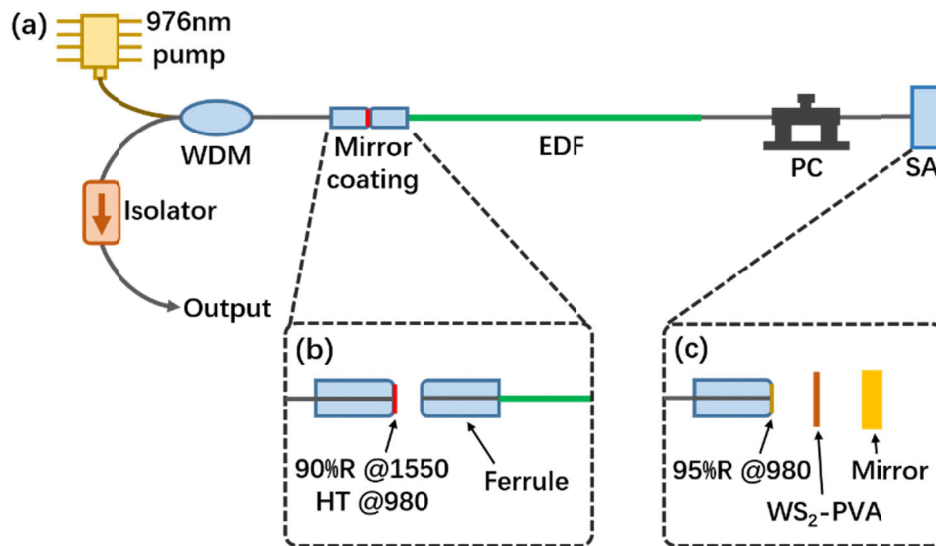

Fig. 2. (a) Laser design. (b) Detailed structure of the left end of the cavity. (c) Detailed structure of the right end of the cavity with WS$_2$-PVA SA. WDM: wavelength division multiplexer; EDF: Erbium-doped fiber; PC: polarization controller; SA: saturable absorber.

The mode locking operation is obtained when the injected pump power is increased to $\sim$250 mW. The mode locking operation becomes unstable when the pump power is further increased up to 390 mW and beyond. The output optical spectrum at the pump power of 350 mW is shown in Fig. 3(a). The central wavelength is 1558.6 nm and the 3-dB bandwidth is 7.4 nm. Kelly sidebands are not observed in the spectrum which is a typical feature for the lasers with short cavity and weak cavity perturbation [29,57,58]. The relation between the injected pump power and the laser output power is provided in Fig. 3(b). The pump power threshold of mode locking operation is $\sim$250 mW which is higher than conventional 2D materials based mode-locked fiber lasers with long cavity. This is because the cavity is short and the cavity dispersion and nonlinearity are both small. As a result, the cavity requires a higher intra-cavity power to initiate the mode locking operation. The slope efficiency is $\sim$2.5%. At a pump power of 350 mW, the output power is 8.7 mW. The maximum output power of mode locking state is $\sim$9 mW, corresponding to a maximum output pulse energy of $\sim$17.2 pJ.
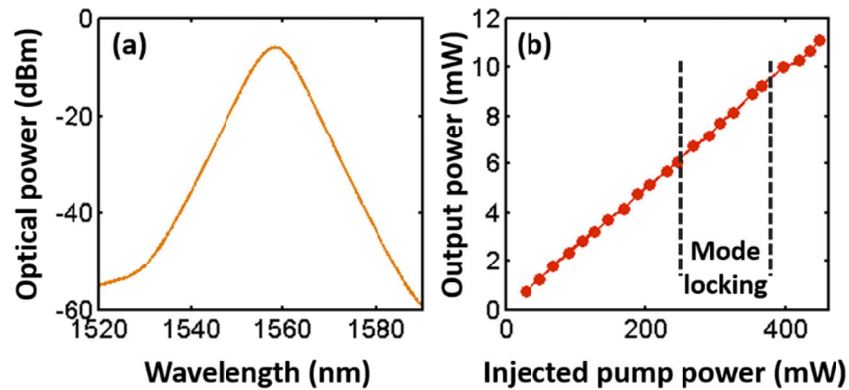
Fig. 3. (a) Optical spectrum. (b) Output power with respect to the injected pump power.

The time-domain properties are then investigated, as shown in Fig. 4. The laser output is measured by a 10-GHz photodetector (EOT 3500F) and a 2-GHz oscilloscope (Agilent DSO9254A). The measured waveform is shown in Fig. 4(a). The period is ~1.9 ns, corresponding to a repetition rate of ~523 MHz. This period is consistent with the round-trip time of the 19.5-cm laser cavity. In the oscilloscope trace, there are some ringing parts after the falling edge of the pulses. They are due to the slight impedance mismatch among the photodetector, cable and oscilloscope. The autocorrelation trace of the output pulse is also measured, as shown in Fig. 4(b). Only a single pulse profile is observed and no bound-state pulses are observed. The autocorrelation trace has a width (FWHM) of 711 fs and is well fitted by a soliton profile ($sech^2$). The corresponding soliton pulse width is 461 fs. The time-bandwidth product is 0.42. The pulse has a negative chirp due to the pigtail fiber outside the laser cavity. In the laser, the WS_2 SA can sustain a few months during the whole experiment, and in each single experiment of ~3 hours the mode locking state can be successfully maintained, which also indicates the good stability of the saturable absorber.
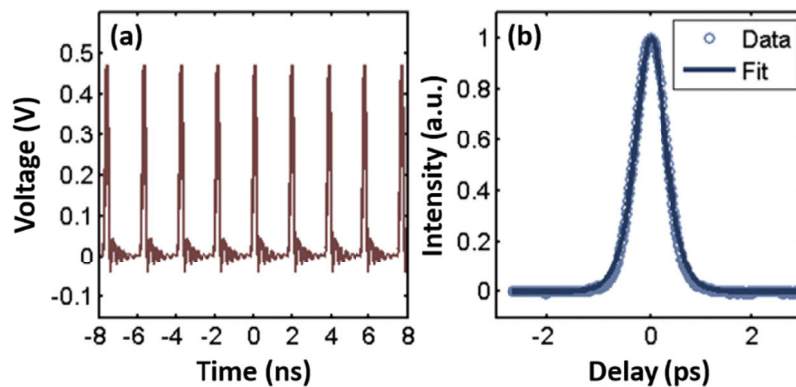

Fig. 4. (a) Oscilloscope trace. (b) Autocorrelation trace and fit.

The frequency-domain properties are also studied, as shown in Fig. 5. The RF spectrum is measured by an RF spectrum analyzer (Keysight N9000B). Figure 5(a) shows the RF spectra near the fundamental frequency of 523 MHz with a span of 10 MHz and a resolution bandwidth (RBW) of 100 Hz. An extinction ratio of ~89 dB is obtained. The inset shows the same spectra with a smaller span of 10 kHz and an RBW of 10 Hz. The RF spectrum up to 5 GHz is presented

in Fig. 5(b). In the whole spectrum, no noise spurious peak is observed which indicates that the laser operates in a stable and low-noise state and has good spectral purity. To further study the timing noise of the laser, the phase noise is measured by a signal source analyzer, as shown in Fig. 6. At offset frequency 1 kHz, the phase noise spectrum value (power spectral density) is ~−115 dBc/Hz. The integrated timing jitter is also calculated based on the phase noise spectrum. It can be found that the timing jitter from 1 kHz to 1 MHz is ~28 fs. Further improvement on the SA nonsaturable loss and coupling efficiency may help to reduce the timing jitter.
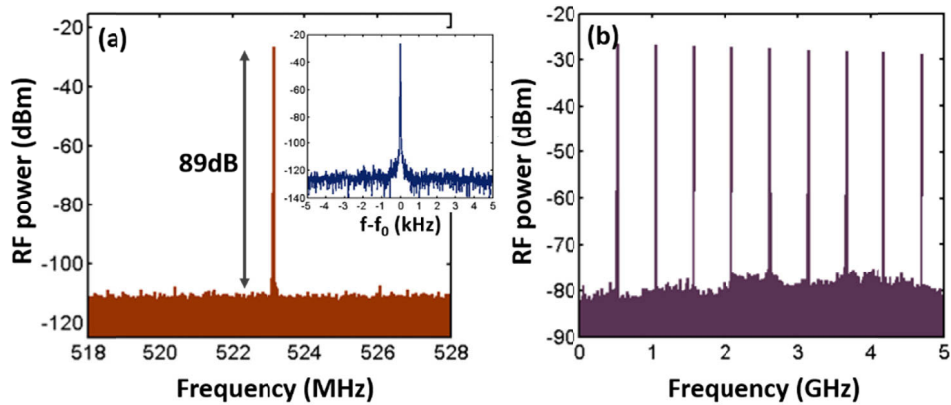
Fig. 5. (a) RF spectrum near 523 MHz with 10 MHz span and 100 Hz RBW. Inset: RF spectrum near 523 MHz with 10 kHz span and 10 Hz RBW. (b) RF spectrum up to 5 GHz.
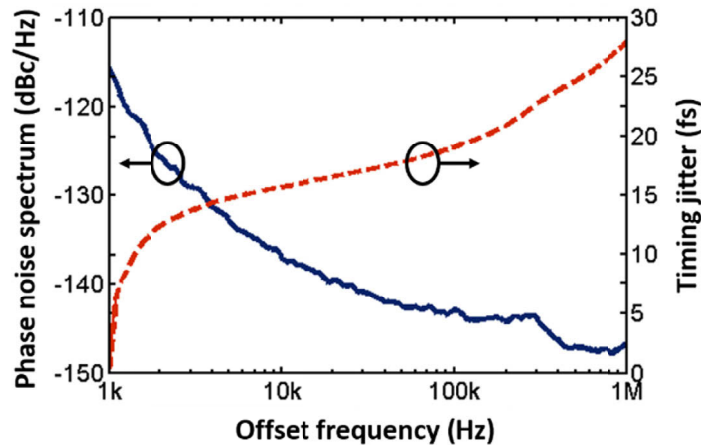

Fig. 6. Phase noise spectrum and timing jitter of the laser.

4. Microwave photonic application

Fundamentally mode-locked lasers provide a high-purity RF spectrum after photodetection, which has the potential in microwave photonic application to generate tunable microwave frequency with high extinction ratio in a wide span. In this section, we use our 523 MHz mode-locked laser to obtain high-purity microwave frequency synthesis from 0.52 GHz to 10.46 GHz.

The experimental setup is shown in Fig. 7(a). A fiber Mach-Zehnder interferometer (MZI) with slightly unequal arm length is constructed. A fiber spool of 16 km fiber is used to provide

high net dispersion and stretch the optical pulses. In the upper arm of MZI, a tunable delay line (TDL) is used to precisely adjust the delay between two arms. In the lower arm, a variable optical attenuator (VOA) and a PC are inserted to balance the loss and control the polarization state between two arms. This structure is also known as a chirp-mixing structure, which performs as a narrow band-pass filter in the microwave domain [62,63].
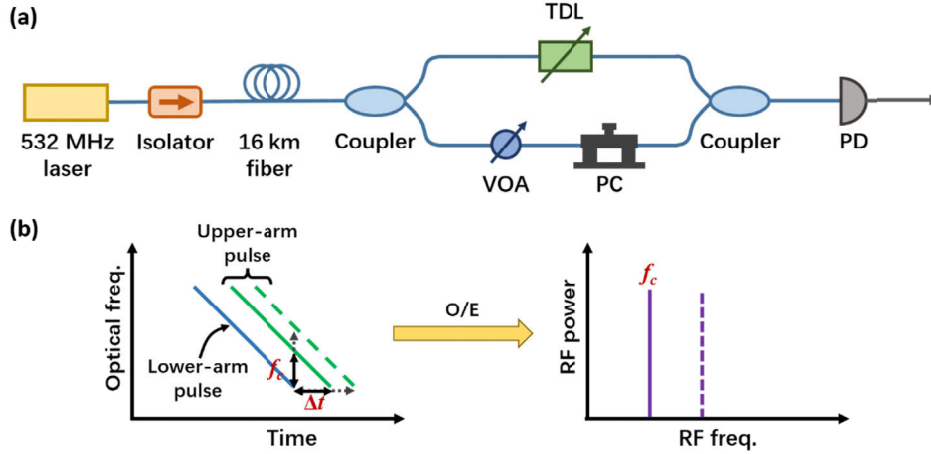
Fig. 7. (a) Experimental setup for microwave generation with 532-MHz mode-locked laser. (b) Principle of microwave generation

The principle can be described by Fig. 7(b). Fiber spool linearly stretches the optical pulses. Then the pulses are split and delayed in the MZI. The left panel in Fig. 7(b) shows the frequency-time map of pulses in the two arms. When they are re-combined after MZI, two optical frequency components overlap in time domain. After photodetection, as shown in the right panel in Fig. 7(b), the beating microwave frequency f_c is equal to the difference between two optical frequencies and its value is determined by the delay between two arms. Therefore f_c is the center frequency of the band-pass filter in microwave frequency domain and is approximately given by [62]

$$f_c \approx \frac{\Delta t}{2\pi |\beta_2| L} \tag{1}$$

where Δt is the delay between two arms, $\beta_2 = -22$ ps^2/km is the second-order dispersion parameter of fiber and $L = 16$ km is the fiber length. By changing the delay, different frequency components can be chosen, shown as the dashed lines in Fig. 7(b). The filter profile (power) is given by [62]

$$\Re(f) \approx \exp\left(-\frac{2\pi^2(\beta_2 L)^2(f - f_c)^2}{\tau_0^2}\right) \tag{2}$$

where f is the microwave frequency and τ_0 is the un-chirped optical pulse width (1/e). With the parameter in our system, the suppression at the closest harmonic frequencies (i.e., $f_c \pm f_{rep}$) is greater than 60 dB. Figure 8 shows a few typical generated microwave spectra at 0.52 GHz, 1.05 GHz, 2.09 GHz, 4.18 GHz, 6.28 GHz, 8.37 GHz and 10.46 GHz, respectively. The spectra have a span from 0 to 11 GHz and a resolution bandwidth of 100 Hz. Very clean spectra can be observed for all these frequencies which indicates good suppression on the unwanted frequency components. If we define an extinction ratio between the power of microwave frequency and the highest noise power within ± 600 MHz span (to cover two closest frequency components to be suppressed), extinction ratios ≥60 dB are obtained for all the frequencies. The extinction ratio values are summarized in Table 1 for all the frequencies.
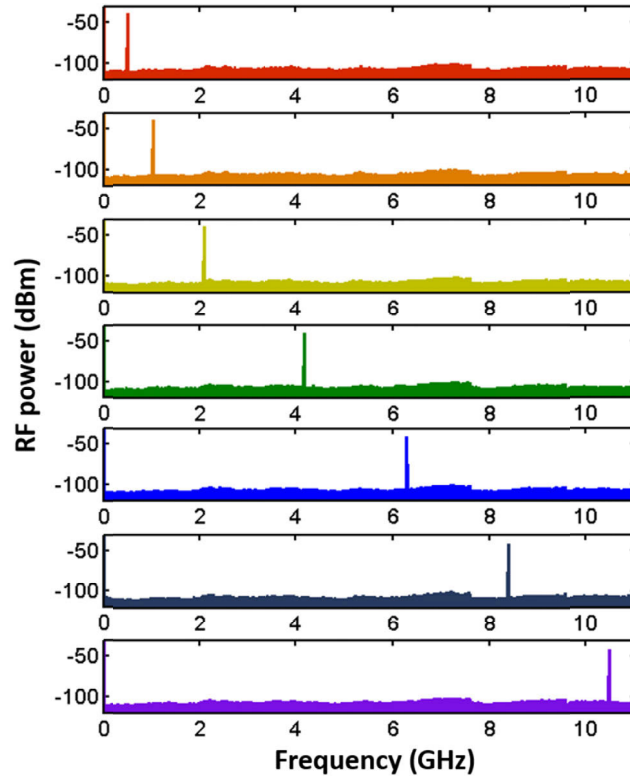
Fig. 8. Typical generated microwave frequencies from 0.52 to 10.46 GHz.

Table 1. Extinction ratio values for the generated microwave frequencies

Freq. (GHz)	Ext. ratio (dB)	Freq. (GHz)	Ext. ratio (dB)
0.52*	67	5.75	63
1.05	67	6.28	60
1.57	64	6.80	60
2.09	63	7.32	60
2.62	63	7.85	60
3.14	64	8.37	63
3.66	63	9.89	62
4.18	63	9.41	62
4.71	65	9.94	62
5.23	63	10.46	62

* The exact frequency is 0.5231 GHz and all the frequencies in the table are integer multiples of this frequency. Only two decimals are shown in the table.

For the mode-locked laser with a repetition rate f_R, the phase noise of the generated microwave frequency at kf_R (k is a positive integer) is related to the phase noise of the laser by [64]

$$S_{ph,m}(\Delta f) = k^2 S_{ph,l}(\Delta f) \tag{3}$$

where $S_{ph,m}$ and $S_{ph,l}$ are the phase noise spectra of the microwave frequency and laser, respectively. Δf is the offset frequency. The measured phase noise spectra of the generated microwave are

shown in Fig. 9(a) following the relation of Eq. (3). The integrated timing jitters (1 kHz – 1 MHz) are shown in Fig. 9(b).
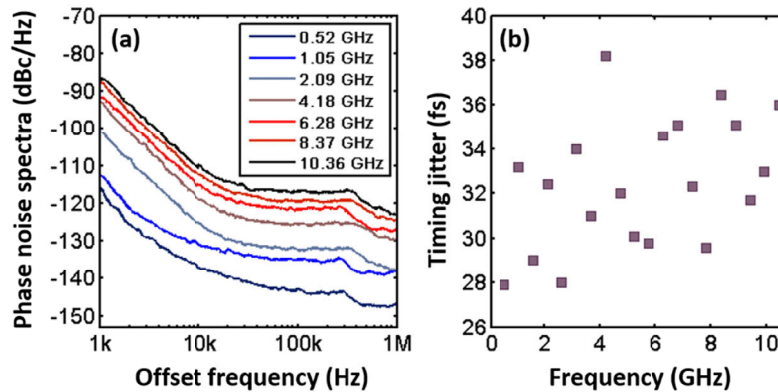
Fig. 9. (a) Phase noise spectra and (b) timing jitters of the microwave frequencies.

5. Conclusions

We have demonstrated a mode-locked Erbium-doped fiber laser with WS_2 saturable absorber and its application in microwave photonic application. The WS_2 SA has a modulation depth of 3.4% and a saturation intensity of ~200 MW/cm^2. The laser operates at fundamental mode locking state with a repetition rate of 523 MHz. The laser has a central wavelength of 1558.6 nm, a 3-dB bandwidth of 7.4 nm and an output power of 8.7 mW. The laser operates at a low-noise state with an extinction ratio of 89 dB in the RF spectrum and a timing jitter of 28 fs (1 kHz – 1 MHz). In the demonstration of high-quality microwave photonic application, high-purity microwave frequencies up to 10.46 GHz have been synthesized with more than 60 dB extinction ratio. Our work indicates the potential of novel 2D material devices such as WS_2 saturable absorber for high-speed and high-precision microwave photonic applications.

Funding

Disclosures

The authors declare no conflicts of interest.

References

1. F. Bonaccorso, Z. Sun, T. Hasan, and A. C. Ferrari, "Graphene photonics and optoelectronics," Nat. Photonics **4**(9), 611–622 (2010).
2. S. Yamashita, "Nonlinear optics in carbon nanotube, graphene, and related 2D materials," APL Photonics **4**(3), 034301 (2019).
3. K. Wu, B. Chen, X. Zhang, S. Zhang, C. Guo, C. Li, P. Xiao, J. Wang, L. Zhou, W. Zou, and J. Chen, "High-performance mode-locked and Q-switched fiber lasers based on novel 2D materials of topological insulators, transition metal dichalcogenides and black phosphorus: review and perspective (invited)," Opt. Commun. **406**, 214–229 (2018).
4. Q. Bao, H. Zhang, Y. Wang, Z. Ni, Y. Yan, Z. X. Shen, K. P. Loh, and D. Y. Tang, "Atomic-Layer Graphene as a Saturable Absorber for Ultrafast Pulsed Lasers," Adv. Funct. Mater. **19**(19), 3077–3083 (2009).

5. M. Liu, R. Tang, A.-P. Luo, W.-C. Xu, and Z.-C. Luo, "Graphene-decorated microfiber knot as a broadband resonator for ultrahigh-repetition-rate pulse fiber lasers," Photonics Res. **6**(10), C1–C7 (2018).

6. B. Yao, G. Soavi, T. Ma, X. Zhang, B. Fu, D. Yoon, S. A. Hussain, A. Lombardo, D. Popa, and A. C. Ferrari, "Gate controllable ultrafast fiber lasers based on graphene," in *Conference on Lasers and Electro-Optics*, OSA Technical Digest (online) (Optical Society of America, 2018), SF3K.6.

7. A. Martinez and S. Yamashita, "10 GHz fundamental mode fiber laser using a graphene saturable absorber," Appl. Phys. Lett. **101**(4), 041118 (2012).

8. J. Sotor, J. Bogusławski, T. Martynkien, P. Mergo, A. Krajewska, A. Przewłoka, W. StrupiŃski, and G. SoboŃ, "All-polarization-maintaining, stretched-pulse Tm-doped fiber laser, mode-locked by a graphene saturable absorber," Opt. Lett. **42**(8), 1592–1595 (2017).

9. Z. Sun, T. Hasan, F. Torrisi, D. Popa, G. Privitera, F. Wang, F. Bonaccorso, D. M. Basko, and A. C. Ferrari, "Graphene Mode-Locked Ultrafast Laser," ACS Nano **4**(2), 803–810 (2010).

10. B. Fu, J. Li, Z. Cao, and D. Popa, "Bound states of solitons in a harmonic graphene-mode-locked fiber laser," Photonics Res. **7**(2), 116–120 (2019).

11. C. A. Zaugg, Z. Sun, V. J. Wittwer, D. Popa, S. Milana, T. S. Kulmala, R. S. Sundaram, M. Mangold, O. D. Sieber, M. Golling, Y. Lee, J. H. Ahn, A. C. Ferrari, and U. Keller, "Ultrafast and widely tuneable vertical-external-cavity surface-emitting laser, mode-locked by a graphene-integrated distributed Bragg reflector," Opt. Express **21**(25), 31548–31559 (2013).

12. I. Baylam, O. Balci, N. Kakenov, C. Kocabas, and A. Sennaroglu, "Graphene-gold supercapacitor as a voltage controlled saturable absorber for femtosecond pulse generation," Opt. Lett. **41**(5), 910–913 (2016).

13. G. Li, Y. Chen, X. Yan, and L. Zhao, "Passive mode locking resulting from weak polarization dependence based on evanescent field interaction with a monolayer graphene absorber," Appl. Opt. **57**(13), 3507–3510 (2018).

14. H. Jeong, S. Y. Choi, M. H. Kim, F. Rotermund, Y.-H. Cha, D.-Y. Jeong, S. B. Lee, K. Lee, and D.-I. Yeom, "All-fiber Tm-doped soliton laser oscillator with 6 nJ pulse energy based on evanescent field interaction with monoloayer graphene saturable absorber," Opt. Express **24**(13), 14152–14158 (2016).

15. X. Li, K. Wu, Z. Sun, B. Meng, Y. Wang, Y. Wang, X. Yu, X. Yu, Y. Zhang, P. P. Shum, and Q. J. Wang, "Single-wall carbon nanotubes and graphene oxide-based saturable absorbers for low phase noise mode-locked fiber lasers," Sci. Rep. **6**(1), 25266 (2016).

16. D. Steinberg, R. M. Gerosa, F. N. Pellicer, J. D. Zapata, S. H. Domingues, E. A. Thoroh de Souza, and L. A. M. Saito, "Graphene oxide and reduced graphene oxide as saturable absorbers onto D-shaped fibers for sub 200-fs EDFL mode-locking," Opt. Mater. Express **8**(1), 144–156 (2018).

17. W. Li, J. Zou, Y. Huang, K. Wang, T. Du, S. Jiang, and Z. Luo, "212-kHz-linewidth, transform-limited pulses from a single-frequency Q-switched fiber laser based on a few-layer Bi2Se3 saturable absorber," Photonics Res. **6**(10), C29–C35 (2018).

18. Z.-C. Luo, M. Liu, H. Liu, X.-W. Zheng, A.-P. Luo, C.-J. Zhao, H. Zhang, S.-C. Wen, and W.-C. Xu, "2 GHz passively harmonic mode-locked fiber laser by a microfiber-based topological insulator saturable absorber," Opt. Lett. **38**(24), 5212–5215 (2013).

19. J. Lee, Y. Kim, K. Lee, and J. H. Lee, "Femtosecond mode-locking of a fiber laser using a CoSb3-skutterudite-based saturable absorber," Photonics Res. **6**(10), C36–C43 (2018).

20. X. Guan, J. Wang, Y. Zhang, B. Xu, Z. Luo, H. Xu, Z. Cai, X. Xu, J. Zhang, and J. Xu, "Self-Q-switched and wavelength-tunable tungsten disulfide-based passively Q-switched Er:Y2O3 ceramic lasers," Photonics Res. **6**(9), 830–836 (2018).

21. W. Liu, M. Liu, M. Lei, S. Fang, and Z. Wei, "Titanium Selenide Saturable Absorber Mirror for Passive Q-Switched Er-Doped Fiber Laser," IEEE J. Sel. Top. Quantum Electron. **24**(3), 1–5 (2018).

22. W. Liu, Y.-N. Zhu, M. Liu, B. Wen, S. Fang, H. Teng, M. Lei, L.-M. Liu, and Z. Wei, "Optical properties and applications for MoS2-Sb2Te3-MoS2 heterostructure materials," Photonics Res. **6**(3), 220–227 (2018).

23. J. Wang, Z. Jiang, H. Chen, J. Li, J. Yin, J. Wang, T. He, P. Yan, and S. Ruan, "High energy soliton pulse generation by a magnetron-sputtering-deposition-grown MoTe2 saturable absorber," Photonics Res. **6**(6), 535–541 (2018).

24. P. Yan, Z. Jiang, H. Chen, J. Yin, J. Lai, J. Wang, T. He, and J. Yang, "α-In2Se3 wideband optical modulator for pulsed fiber lasers," Opt. Lett. **43**(18), 4417–4420 (2018).

25. R. I. Woodward, E. J. R. Kelleher, R. C. T. Howe, G. Hu, F. Torrisi, T. Hasan, S. V. Popov, and J. R. Taylor, "Tunable Q-switched fiber laser based on saturable edge-state absorption in few-layer molybdenum disulfide (MoS2)," Opt. Express **22**(25), 31113–31122 (2014).

26. D. Mao, X. Cui, X. Gan, M. Li, W. Zhang, H. Lu, and J. Zhao, "Passively Q-Switched and Mode-Locked Fiber Laser Based on an ReS2 Saturable Absorber," IEEE J. Sel. Top. Quantum Electron. **24**(3), 1–6 (2018).

27. D. Mao, Y. Wang, C. Ma, L. Han, B. Jiang, X. Gan, S. Hua, W. Zhang, T. Mei, and J. Zhao, "WS2 mode-locked ultrafast fiber laser," Sci. Rep. **5**(1), 7965 (2015).

28. R. Khazaeizhad, S. H. Kassani, H. Jeong, D.-I. Yeom, and K. Oh, "Mode-locking of Er-doped fiber laser using a multilayer MoS2 thin film as a saturable absorber in both anomalous and normal dispersion regimes," Opt. Express **22**(19), 23732–23742 (2014).

29. K. Wu, X. Zhang, J. Wang, and J. Chen, "463-MHz fundamental mode-locked fiber laser based on few-layer MoS2 saturable absorber," Opt. Lett. **40**(7), 1374–1377 (2015).

30. K. Wang, J. Wang, J. Fan, M. Lotya, A. O'Neill, D. Fox, Y. Feng, X. Zhang, B. Jiang, Q. Zhao, H. Zhang, J. N. Coleman, L. Zhang, and W. J. Blau, "Ultrafast Saturable Absorption of Two-Dimensional MoS2 Nanosheets," ACS Nano **7**(10), 9260–9267 (2013).

31. G. Wang, G. Liang, A. A. Baker-Murray, K. Wang, J. J. Wang, X. Zhang, D. Bennett, J.-T. Luo, J. Wang, P. Fan, and W. J. Blau, "Nonlinear optical performance of few-layer molybdenum diselenide as a slow-saturable absorber," Photonics Res. **6**(7), 674–680 (2018).

32. M. Zhang, Q. Wu, F. Zhang, L. Chen, X. Jin, Y. Hu, Z. Zheng, and H. Zhang, "2D Black Phosphorus Saturable Absorbers for Ultrafast Photonics," Adv. Opt. Mater. **7**(1), 1800224 (2019).

33. R. I. Woodward, M. R. Majewski, N. Macadam, G. Hu, T. Albrow-Owen, T. Hasan, and S. D. Jackson, "Q-switched Dy:ZBLAN fiber lasers beyond 3 µm: comparison of pulse generation using acousto-optic modulation and inkjet-printed black phosphorus," arXiv, 1902.06945 (2019).

34. J. Sotor, G. Sobon, M. Kowalczyk, W. Macherzynski, P. Paletko, and K. M. Abramski, "Ultrafast thulium-doped fiber laser mode locked with black phosphorus," Opt. Lett. **40**(16), 3885–3888 (2015).

35. G. Hu, T. Albrow-Owen, X. Jin, A. Ali, Y. Hu, R. C. T. Howe, K. Shehzad, Z. Yang, X. Zhu, R. I. Woodward, T.-C. Wu, H. Jussila, J.-B. Wu, P. Peng, P.-H. Tan, Z. Sun, E. J. R. Kelleher, M. Zhang, Y. Xu, and T. Hasan, "Black phosphorus ink formulation for inkjet printing of optoelectronics and photonics," Nat. Commun. **8**(1), 278 (2017).

36. J. Li, H. Luo, B. Zhai, R. Lu, Z. Guo, H. Zhang, and Y. Liu, "Black phosphorus: a two-dimension saturable absorption material for mid-infrared Q-switched and mode-locked fiber lasers," Sci. Rep. **6**(1), 30361 (2016).

37. Z. Qin, T. Hai, G. Xie, J. Ma, P. Yuan, L. Qian, L. Li, L. Zhao, and D. Shen, "Black phosphorus Q-switched and mode-locked mid-infrared Er:ZBLAN fiber laser at 3.5 µm wavelength," Opt. Express **26**(7), 8224–8231 (2018).

38. X. Jiang, S. Liu, W. Liang, S. Luo, Z. He, Y. Ge, H. Wang, R. Cao, F. Zhang, Q. Wen, J. Li, Q. Bao, D. Fan, and H. Zhang, "Broadband Nonlinear Photonics in Few-Layer MXene Ti3C2Tx (T = F, O, or OH)," Laser Photonics Rev. **12**(2), 1700229 (2018).

39. Y. Meng, C. Zhu, Y. Li, X. Yuan, F. Xiu, Y. Shi, Y. Xu, and F. Wang, "Three-dimensional Dirac semimetal thin-film absorber for broadband pulse generation in the near-infrared," Opt. Lett. **43**(7), 1503–1506 (2018).

40. Y. I. Jhon, J. Koo, B. Anasori, M. Seo, J. H. Lee, Y. Gogotsi, and Y. M. Jhon, "Metallic MXene Saturable Absorber for Femtosecond Mode-Locked Lasers," Adv. Mater. **29**(40), 1702496 (2017).

41. C. Zhu, F. Wang, Y. Meng, X. Yuan, F. Xiu, H. Luo, Y. Wang, J. Li, X. Lv, L. He, Y. Xu, J. Liu, C. Zhang, Y. Shi, R. Zhang, and S. Zhu, "A robust and tuneable mid-infrared optical switch enabled by bulk Dirac fermions," Nat. Commun. **8**(1), 14111 (2017).

42. Z. H. Hui, W. Xu, X. L. Li, P. Guo, Y. Z. Zhang, and J. Liu, "Cu2S nanosheets for ultrashort pulse generation in the near-infrared region," Nanoscale **11**(13), 6045–6051 (2019).

43. S. Hong, F. Lédée, J. Park, S. Song, H. Lee, Y. S. Lee, B. Kim, D.-I. Yeom, E. Deleporte, and K. Oh, "Mode-Locking of All-Fiber Lasers Operating at Both Anomalous and Normal Dispersion Regimes in the C- and L-Bands Using Thin Film of 2D Perovskite Crystallites," Laser Photonics Rev. **12**(11), 1800118 (2018).

44. W. Li, J. Peng, Y. Zhong, D. Wu, H. Lin, Y. Cheng, Z. Luo, J. Weng, H. Xu, and Z. Cai, "Orange-light passively Q-switched Pr3+-doped all-fiber lasers with transition-metal dichalcogenide saturable absorbers," Opt. Mater. Express **6**(6), 2031–2039 (2016).

45. A. Malouf, O. Henderson-Sapir, S. Set, S. Yamashita, and D. J. Ottaway, "Two-photon absorption and saturable absorption of mid-IR in graphene," Appl. Phys. Lett. **114**(9), 091111 (2019).

46. K. Wu, Y. Wang, C. Qiu, and J. Chen, "Thermo-optic all-optical devices based on two-dimensional materials," Photonics Res. **6**(10), C22–C28 (2018).

47. K. Wu, C. Guo, H. Wang, X. Zhang, J. Wang, and J. Chen, "All-optical phase shifter and switch near 1550 nm using tungsten disulfide (WS2) deposited tapered fiber," Opt. Express **25**(15), 17639–17649 (2017).

48. X. Yang, Q. Long, Z. Liu, Y. Zhang, J. Yang, D. Kong, L. Yuan, and K. Oh, "Microfiber interferometer integrated with Au nanorods for an all-fiber phase shifter and switch," Opt. Lett. **44**(5), 1092–1095 (2019).

49. S. Yu, X. Wu, K. Chen, B. Chen, X. Guo, D. Dai, L. Tong, W. Liu, and Y. Ron Shen, "All-optical graphene modulator based on optical Kerr phase shift," Optica **3**(5), 541–544 (2016).

50. W. Li, B. Chen, C. Meng, W. Fang, Y. Xiao, X. Li, Z. Hu, Y. Xu, L. Tong, H. Wang, W. Liu, J. Bao, and Y. R. Shen, "Ultrafast All-Optical Graphene Modulator," Nano Lett. **14**(2), 955–959 (2014).

51. Q. Wu, S. Chen, Y. Wang, L. Wu, X. Jiang, F. Zhang, X. Jin, Q. Jiang, Z. Zheng, J. Li, M. Zhang, and H. Zhang, "MZI-Based All-Optical Modulator Using MXene Ti3C2Tx (T = F, O, or OH) Deposited Microfiber," Adv. Mater. Technol. **4**(4), 1800532 (2019).

52. X. Gan, C. Zhao, Y. Wang, D. Mao, L. Fang, L. Han, and J. Zhao, "Graphene-assisted all-fiber phase shifter and switching," Optica **2**(5), 468–471 (2015).

53. P. Xiao, K. Wu, D. Mao, and J. Chen, "A pulsewidth measurement technology based on carbon-nanotube saturable absorber," Opt. Express **27**(4), 4188–4203 (2019).

54. A. Khilo, S. J. Spector, M. E. Grein, A. H. Nejadmalayeri, C. W. Holzwarth, M. Y. Sander, M. S. Dahlem, M. Y. Peng, M. W. Geis, N. A. DiLello, J. U. Yoon, A. Motamedi, J. S. Orcutt, J. P. Wang, C. M. Sorace-Agaskar, M. A. Popović, J. Sun, G.-R. Zhou, H. Byun, J. Chen, J. L. Hoyt, H. I. Smith, R. J. Ram, M. Perrott, T. M. Lyszczarz, E. P. Ippen, and F. X. Kärtner, "Photonic ADC: overcoming the bottleneck of electronic jitter," Opt. Express **20**(4), 4454–4469 (2012).

55. G. Yang, W. Zou, Y. Yuan, and J. Chen, "Wideband signal detection based on high-speed photonicanalog-to-digital converter," Chin. Opt. Lett. **16**(3), 030601 (2018).

56. G. Yang, W. Zou, L. Yu, N. Qian, and J. Chen, "Investigation of electronic aperture jitter effect in channel-interleaved photonic analog-to-digital converter," Opt. Express **27**(6), 9205–9214 (2019).

57. C. Kim, D. Kim, Y. Cheong, D. Kwon, S. Y. Choi, H. Jeong, S. J. Cha, J.-W. Lee, D.-I. Yeom, F. Rotermund, and J. Kim, "300-MHz-repetition-rate, all-fiber, femtosecond laser mode-locked by planar lightwave circuit-based saturable absorber," Opt. Express **23**(20), 26234–26242 (2015).

58. H. Byun, M. Y. Sander, A. Motamedi, H. Shen, G. S. Petrich, L. A. Kolodziejski, E. P. Ippen, and F. X. Kärtner, "Compact, stable 1 GHz femtosecond Er-doped fiber lasers," Appl. Opt. **49**(29), 5577–5582 (2010).

59. J. Zhang, Z. Kong, Y. Liu, A. Wang, and Z. Zhang, "Compact 517 MHz soliton mode-locked Er-doped fiber ring laser," Photonics Res. **4**(1), 27–29 (2016).

60. K. Wu, X. Li, Y. Wang, Q. J. Wang, P. P. Shum, and J. Chen, "Towards low timing phase noise operation in fiber lasers mode locked by graphene oxide and carbon nanotubes at 1.5 µm," Opt. Express **23**(1), 501–511 (2015).

61. A. Berkdemir, H. R. Gutiérrez, A. R. Botello-Méndez, N. Perea-López, A. L. Elías, C.-I. Chia, B. Wang, V. H. Crespi, F. López-Urías, J.-C. Charlier, H. Terrones, and M. Terrones, "Identification of individual and few layers of WS2 using Raman Spectroscopy," Sci. Rep. **3**(1), 1755 (2013).

62. J. Wong, H. Q. Lam, S. Aditya, K. E. K. Lee, V. Wong, P. H. Lim, K. Wu, C. Ouyang, and P. P. Shum, "Photonic Generation of Tunable Continuous-Wave Microwave Signals Using a Temporally-Stretched and Chirped Pulse-Train," J. Lightwave Technol. **30**(9), 1269–1277 (2012).

63. H. Zhang, W. Zou, and J. Chen, "Generation of a widely tunable linearly chirped microwave waveform based on spectral filtering and unbalanced dispersion," Opt. Lett. **40**(6), 1085–1088 (2015).

64. D. von der Linde, "Characterization of the noise in continuously operating mode-locked lasers," Appl. Phys. B: Lasers Opt. **39**(4), 201–217 (1986).